Appl. Phys. A (2006)
DOI: 10.1007/s00339-006-3570-8

Applied Physics A
Materials Science & Processing

E. PERELLI-CIPPO[1,✉]
G. GORINI[1]
M. TARDOCCHI[1]
C. ANDREANI[2]
A. PIETROPAOLO[2]
R. SENESI[2]
N.J. RHODES[3]
E.M. SCHOONEVELD[3]

The O–H stretching band in ice Ih derived via eV neutron spectroscopy on VESUVIO using the new very low angle detector bank

[1] Universita' degli Studi di Milano-Bicocca and CNR-INFM, UdR Milano-Bicocca, Italy
[2] Universita' degli Studi di Roma – Tor Vergata and CNR-INFM, UdR Tor Vergata, Italy
[3] ISIS Pulsed Neutron Source – Rutherford-Appleton Laboratory, Chilton, UK

Received: 28 November 2005 / Accepted: 13 February 2006

ABSTRACT Strong demand exists for an experimental facility enabling new experimental investigations on condensed matter systems based on epithermal neutron scattering at high energy and low momentum transfers. This need will be met by the very low angle detector (VLAD) bank, to be installed on the VESUVIO spectrometer at the ISIS spallation neutron source. The equipment will operate in the scattering angular range $1^\circ < 2\theta < 5^\circ$. Scattering measurements from a polycrystalline ice sample using a VLAD prototype demonstrates the effectiveness of the detection technique adopted for the construction of the full detector array. The resulting density of states in ice is 9 ± 2 atoms/cell, in agreement with previous measurements.

PACS 61.12.Ex; 63.20.Dj; 63.50.+x

1 Introduction

Strong demand exists for detection systems for neutrons of high energy transfer coupled to low momentum transfer to enable new experimental investigations on condensed matter systems. The provision of equipment for a high energy inelastic neutron scattering (HINS) regime on the VESUVIO spectrometer would allow experimental studies in areas such as the dispersion relations of high energy excitations in metals and compounds [1, 2], molecular electronic excitations and electronic levels in semiconductors [3] and magnetic materials [4]. Such a facility would provide access to the unexplored kinematical regions of (q, ω) space (i.e. $q < 10\,\text{Å}^{-1}$, $500\,\text{meV} < \hbar\omega < 5\,\text{eV}$) and would complement the current deep inelastic neutron scattering (DINS) regime where, with $\hbar\omega > 1$ eV coupled to a wave-vector range $20\,\text{Å}^{-1} < q < 250\,\text{Å}^{-1}$, it is possible to probe the short time single particle dynamics, the momentum distribution, $n(p)$, and the mean kinetic energy, $\langle E_\text{K} \rangle$, in quantum and molecular systems.

It is well known that the combined HINS requirements of high ω and low q are achieved in neutron spectroscopy through the use of very high incident energies coupled with very small scattering angles. On VESUVIO this translates into the need to detect neutrons of tens of eV at a scattering angular range of $1^\circ < 2\theta < 5^\circ$. Accordingly the spectrometer has been modified by narrowing the neutron beam collimation and by fitting a new vacuum vessel, providing minimum attenuation of the neutrons scattered at low angles. More important is the recent development of the resonance detector (RD), which exploits resonance radiative neutron capture in a thin uranium foil for energy analysis of the neutrons. The detection of the photon cascade following neutron capture is done with yttrium aluminium perovskite (YAP) scintillators coupled to a photo multiplier tube and provides the neutron time of flight (TOF).

The RD technology has been selected for the design of the very low angle detector (VLAD), which is due for construction, installation and commissioning (by December 2005) on VESUVIO [5]. The final VLAD design will be similar to the one shown in the model of Fig. 1: a number of detectors, segmented for optimal light collection and spatial resolution, will cover the angular range $1^\circ - 5^\circ$ at a distance of about 2 m from the scattering sample.

The feasibility of VLAD has been investigated by building a prototype detector bank consisting of four RD detectors. The detector bank has been used to record scattering off a polycrystalline ice sample. The resulting absolute scattering function $S(q, \omega)$ features a peak (at $\hbar\omega \cong 420\,\text{meV}$) due to O–H stretching which can be further analyzed bearing in mind that in a polycrystalline sample $S(q, \omega)$ can be expressed in terms of its $q \to 0$ limit. The results of the experiment, and the ensuing data analysis leading to the determination of $g(\omega)$, are presented in this paper.

2 Experiment

2.1 *Experimental set up*

VESUVIO is an inverse geometry TOF spectrometer [6], where the final energy of the neutron is fixed, and the initial one is related to the time of flight via [7]:

$$t = \frac{L_0}{\sqrt{\frac{2E_0}{m}}} + \frac{L_1}{\sqrt{\frac{2E_1}{m}}} + t_c, \tag{1}$$

where t is the time position in the TOF spectrum, t_c is an instrumental offset, E_0 and E_1 are the neutron initial and final energies, L_0 and L_1 are the primary and secondary flight

✉ Fax: +39 0264482505, E-mail: enrico.perelli@mib.infn.it

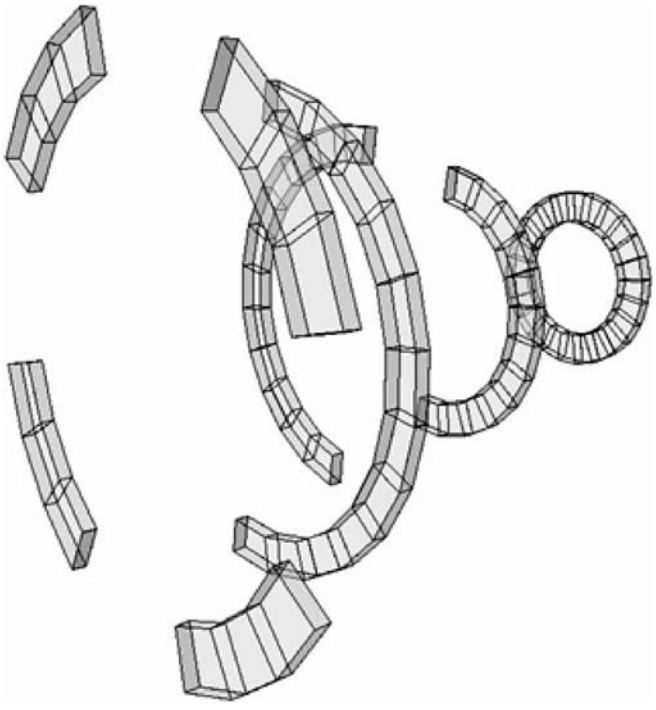

FIGURE 1 A possible configuration of the VLAD detector bank presently under construction. Only the scintillating crystals are shown. The crystals are arranged to cover half rings around the unscattered neutron beam. The angular range covered is $1° < 2\theta < 3°$

paths and m is the neutron mass. Figure 2 shows a schematic layout of the experimental set up for the VLAD measurements on VESUVIO. In order to perform HINS measurements, VESUVIO was equipped with three new components: an insert collimator, an extended vacuum vessel and a prototype detector bank. The collimator is composed of three boron carbide (B_4C) hollow cylinders (see Fig. 3) of about 250 mm length, placed in the incoming neutron beam pipe. Inner diameters are 26 mm, 24 mm, and 22 mm, decreasing in the sample direction. The collimator reduces the divergence of the neutron penumbra in order to both improve the angular resolution [8] and prevent the transmitted beam from hitting the neutron detectors. The neutron penumbra diameter at the sample position is about 23 mm, and about 45 mm at the detector position; this is comfortably less than the vacuum pipe diameter at the detector position, which is about 100 mm.

An extended vacuum vessel is installed between the sample and the detectors; it allows the scattered neutrons to travel in vacuum all the way to the detectors, except for a thin aluminium window at the detector region; this has a thickness of 1 mm apart from six reinforcement beams of 5 mm thickness.

Presently the detector bank is composed of four RD units shown in Fig. 4. Each unit is made of a pair of YAP scintillator crystals coupled to uranium foils of 25 μm thickness. The crystals are of trapezoidal shape, with 46 mm and 40 mm bases, 25 mm height and 6 mm thick. The shape was chosen in order to be well matched to the 5° ring of detectors proposed for the final detector array. Each crystal pair is optically coupled to a 38 mm PM tube via a reflecting aluminium light guide. Two of the four RD in the VLAD prototype are positioned at an angle of 5°. The other two can be moved in the range $2° - 5°$ and were positioned at 2° and 3.5° for these measurements so as to collect data at three different angular positions.

2.2 RD *parameters and optimization*

The optimized use of YAP crystals for RD devices is discussed in [9], to which we refer for details. Essential for achieving a good signal to background ratio (S/B) is the use of a suitable lower level discrimination threshold (LLD) so as to discard a significant fraction of the γ background. A strong background component comes from ^{10}B, a common material in neutron collimation and shielding in the experimental hall. Following neutron capture in ^{10}B, a characteristic 480 keV γ is emitted. By comparison a total energy of about 4 MeV is released following neutron absorption in ^{238}U. Hence for these measurements a LLD at 600 keV equivalent photon energy was set in order to reject the background γ emission from boron-rich materials.

The crystal thickness of 6 mm is a good compromise between the need for high detection efficiency, which would require a large thickness, and the need for a good S/B and a low rate of multiple events (such as cross-talk between detectors and neutron scattering inside the detectors [10]). This can be understood by noting that the signal detection efficiency tends to saturate as the crystal thickness is increased. Quantitatively a statistical figure of merit F can be used to determine the optimal crystal thickness. F was introduced in [11] as the reciprocal of the relative statistical error on the number of counts under a signal peak:

$$F = \left(\frac{\sigma_S}{S}\right)^{-1} . \tag{2}$$

This can be derived from the total rate $S + B$ and expressed in terms of S/B as [11]

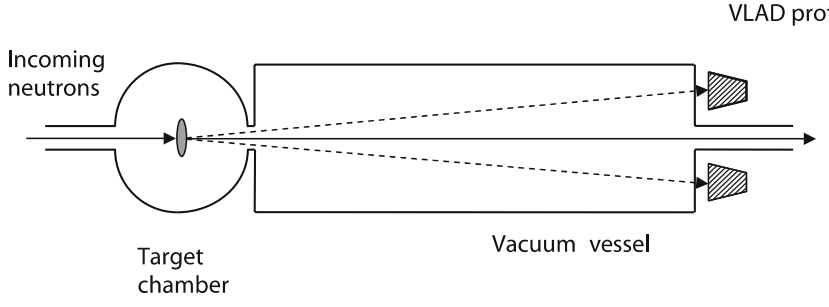

FIGURE 2 Schematics of the VESUVIO spectrometer showing the location of the VLAD prototype detectors behind the extended vacuum vessel. The incoming neutron beam is collimated before hitting the sample placed inside an aluminium vacuum chamber at a distance $L_0 = 11.055$ m from the moderator. The distance between the sample and the VLAD detectors is $L_1 = 2.01$ m

FIGURE 3 Photograph of the three boron carbide hollow cylinders used for the insert collimator

$$F = \frac{S/B}{\sqrt{\left(1+S/B\right)\left(2+S/B\right)}}\sqrt{\varepsilon}, \tag{3}$$

where $\varepsilon = S + B$. This reduces to the well known $F \approx \sqrt{S}$ in the limit $S >> B$. In the VLAD case the opposite limit applies, and F is approximately given by:

$$F = \frac{S}{\sqrt{2B}}. \tag{4}$$

Equation (4) provides a convenient expression for estimates of F and its dependence on the detector thickness. To this aim S can be determined from the signal detection efficiency η, defined as the fraction of photons emitted isotropically by the uranium foil leading to a detected signal in the YAP scintillators. η was determined with the help of Monte Carlo simulations using the GEANT4 package as described in [10]. The η value for crystal thicknesses of 6 and 12 mm and for photon energy of 1 MeV is found to be 10.2% and 14.3%, respectively. Assuming that the background scales proportionally to the scintillator volume, F is practically the same for 6 mm and 12 mm. Thus there would be no advantage in using a thicker YAP scintillator. On the other hand, if the scintillator thickness is decreased from 6 mm to 3 mm, both S and B decrease with the scintillator volume and a worse figure of merit F is found. In conclusion, the thickness of 6 mm is close to optimum in terms of signal quality of the VLAD measurements.

The above values of the detection efficiency η were computed with the GEANT4 code assuming the LLD threshold of 600 keV used in the measurements. The effect of the LLD on the figure of merit F was discussed in [11], where it was found that F has a broad plateau above 600 keV; i.e., raising the threshold above this value does not change the F value significantly.

2.3 *Measurements*

The scattering measurements were performed on a water sample at 270 K (ice Ih). Several neutron and Raman scattering investigations of ice are available (such as for example in [12, 13]). It thus represents a suitable benchmark for HINS measurements. The sample was contained inside a 1 mm thick and 50 mm wide aluminium cell, and its temperature was remotely controlled by means of two sensors, providing a sensitivity of 0.1 K.

FIGURE 4 Photograph of the VLAD prototype installed on VESUVIO. The four RD units are attached to a common frame and view the sample through the thin aluminium window of the extended vacuum vessel

The experimental signal recorded by each VLAD detector is a TOF spectrum, representing the number of counts collected in a time channel of width δt centred in t. Figures 5–7 show the normalised spectra collected in this experiment in the region 50–450 μs. The bottom graph in each figure represents the scattering spectrum from the empty container which provides a direct measurement of part of the background, while the top one is the same spectrum from the H_2O sample+container. Dashed vertical lines at 360 μs, 200 μs, 150 μs and 110 μs mark the elastic scattering contributions, corresponding to final neutron energies equal to the four ^{238}U resonances listed in Table 1. Determining the shape and intensity of the H peaks is the objective of the measurements where the main problem is to discriminate these (signal) peaks from everything else (background). The main background component is a continuum (see below). Other background components appear in the form of peaks such as those due to neutrons scattering off aluminium and oxygen. These peaks overlap with the main component of the H elastic peak, but not with the inelastic peaks due to the O–H stretching band in H_2O, which is investigated in these measurements. The intensity of the

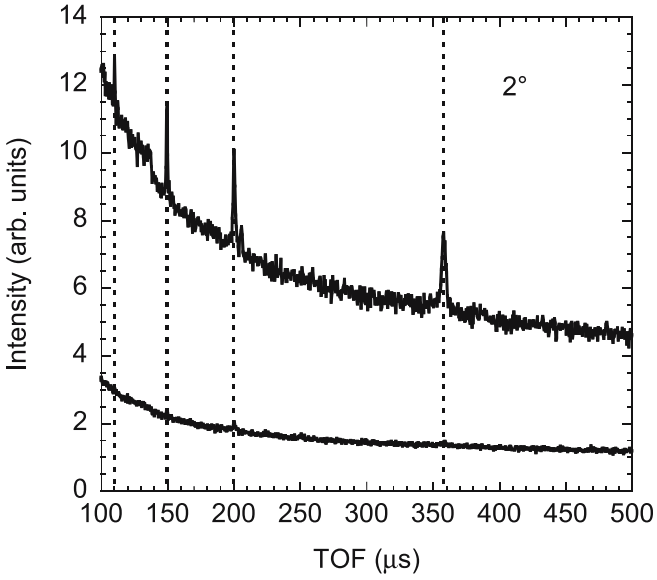

FIGURE 5 Experimental TOF spectra from the empty Al container (bottom) and from the ice+container sample (top) for the VLAD detector at $2\theta = 2°$. The vertical lines mark the position of the four elastic scattering peaks, corresponding to the four absorption resonances of ^{238}U

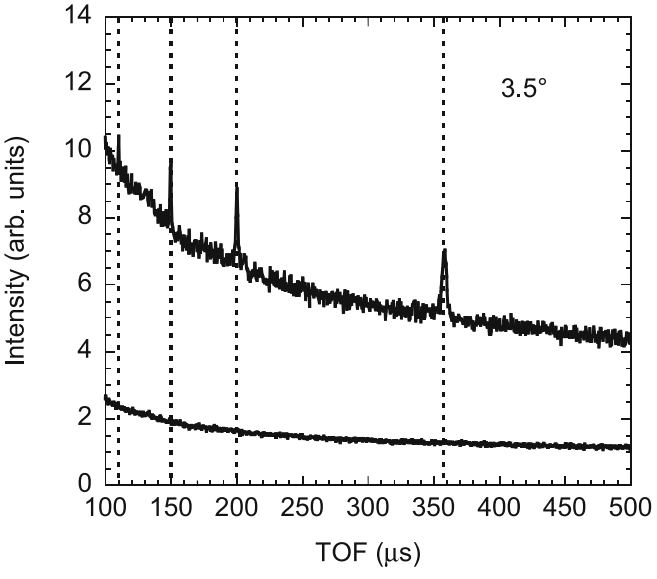

FIGURE 6 Same as Figure 5 but with the detector at 3.5°

Al contribution is determined from the measurements with the empty container. Visual inspection of Figs. 5–7 shows that this contribution is quite small and can be neglected in the analysis. The oxygen contribution cannot be measured independently but the ^{16}O neutron scattering cross section at eV energies is known to be about 20 times smaller than the H cross section. Thus the contamination of the H signal peaks from peaks due to other elements is negligible in these measurements. The only background component that must be subtracted carefully from the data before analysis is the continuum.

The continuum background component is essentially due to the following effects: 1) uranium natural radioactivity and 2) neutron-induced radioactivity. The first component is independent of the flight time and can be determined from

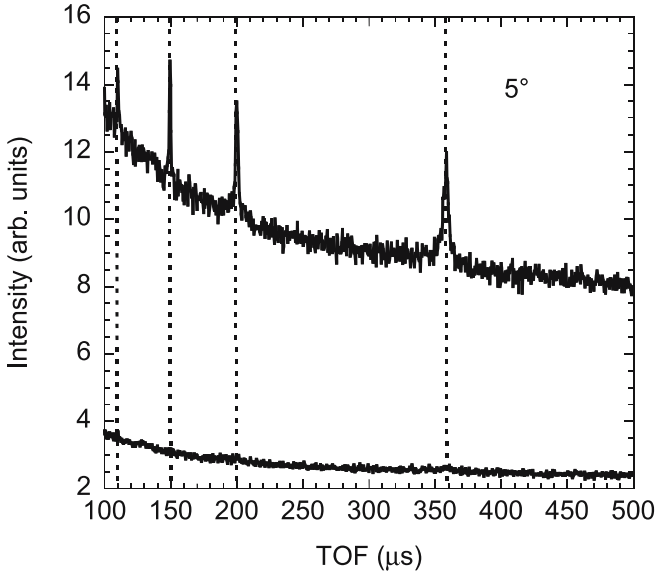

FIGURE 7 Same as Fig. 5 but with the detector at 5°

TABLE 1 Main parameters for the first four resonances in ^{238}U. E_1 is the resonance energy, σ_0 is the nuclear resonance cross-section, Γ is the Breit–Wigner nuclear resonance width, Δ is the width (standard deviation) of the Gaussian broadening due to thermal motion of the absorbing nuclei at a temperature of 295 K, and σ_{eff} is the resulting effective resonance cross-section.

E_1 [eV]	σ_0 [barn]	Γ[meV]	σ_{eff} [barn]
6.671	23564	25	7570
20.87	37966	34	9864
36.68	42228	57	13363
66.02	20134	48	4357

the asymptotic behaviour of the TOF spectrum at long TOF values (i.e. 10–20 ms). The neutron-induced background amounts to a large fraction of the total background under the signal peaks. Since it is sample dependent, it can only be determined from shape information in between the H recoil peaks. This piece of information is achieved by fitting an analytical function to the background, which is then used to interpolate the background underneath the recoil peaks. Care must be taken in excluding from the fit the recoil peak wings, where the inelastic scattering contributions are expected.

The following functional form has been fitted to the background continuum in the time intervals between the recoil peaks:

$$I(t) = A_0 + A_1 t^{-A_2} + A_3 t^{-A_4}. \tag{5}$$

Here t is the neutron TOF, while A_i $(i = 0, 4)$ are fitting parameters determined by a χ-square minimization procedure. The fitting function is shown as a full line in Fig. 8. The same fit was performed on the TOF spectrum from the empty cell. Subtraction of the fitted background continuum leads to the TOF spectra shown in Figs. 8–10. Only the peaks corresponding to a final neutron energy of 6.67 eV are shown. The other peaks, although visible in Figs. 5–7, lack the required resolution and statistics to be useful for investigating the scattering contribution from vibrational bands. The position of

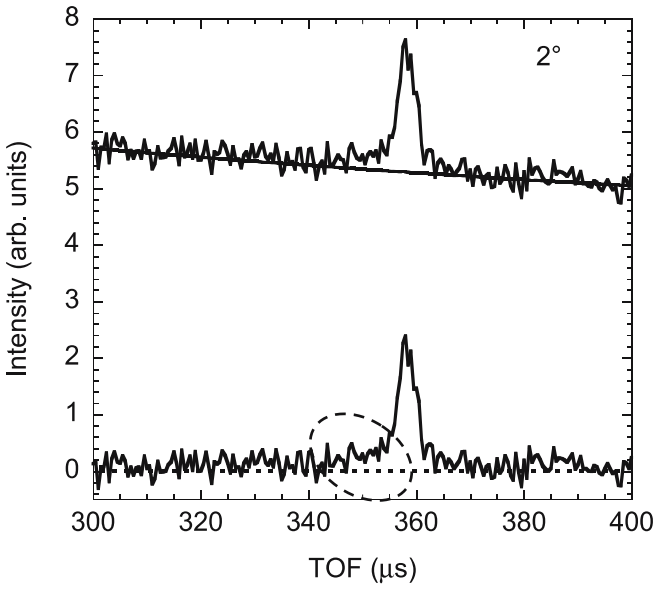

FIGURE 8 TOF spectrum for the $2\theta = 2°$ detector in the region of the first ^{238}U resonance. In the top graph the raw data are shown together with the interpolated background curve. Subtraction of the interpolated background leads to the data in the bottom spectrum. The region of interest for observing the inelastic peak due to the O–H stretching band is on the left of the main H recoil peak

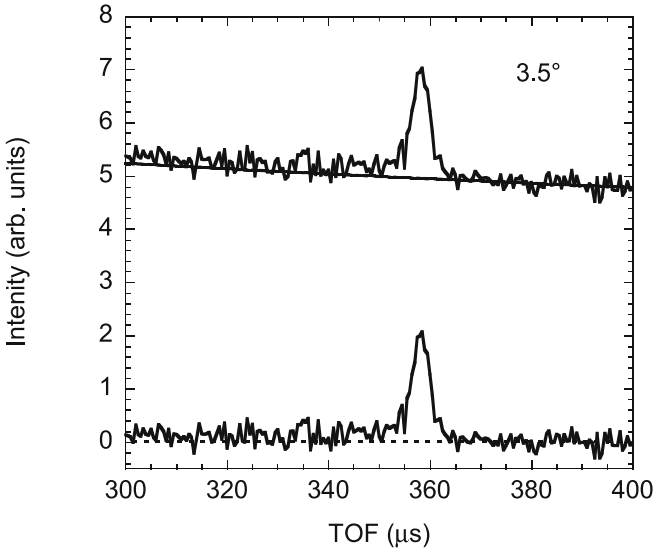

FIGURE 9 Same as Fig. 8 but with the detector at $2\theta = 3.5°$

these peaks has only been used for instrumental calibration (i.e. for determining electronic time offsets and accurate determination of the L_1 flight path) as explained in [14]. The full set of calibrated instrumental parameters used in the analysis is summarised in Table 2.

The data of Figs. 8–10 contain the physical information on the inelastic neutron scattering cross section of hydrogen in the ice sample; indeed the count rate of the detectors is proportional to the double differential cross section $\frac{\partial^2\sigma}{\partial\Omega\partial E_1}$ and to the dynamic structure factor $S(q,\omega)$, as shown below. The region of the O–H stretching band is on the left hand side of the main recoil peak, at a distance of about 10 μs. Despite the limited statistics of these prototype measurements, a peak is observed in the region marked with a circle in Fig. 8. This peak can be further analysed as explained below.

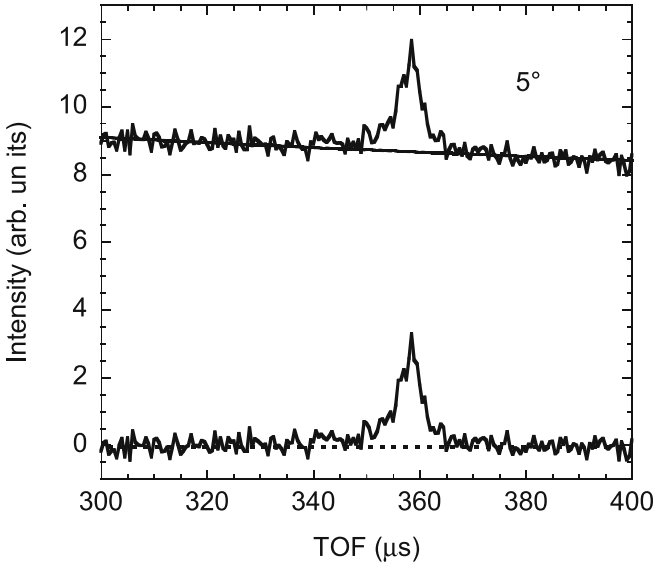

FIGURE 10 Same as Fig. 8 but with the detector at $2\theta = 5°$

TABLE 2 Instrumental parameters of the VESUVIO spectrometer with the installation of the VLAD detector. L_0 and L_1 are the incoming and scattered neutron flight paths, 2θ is the scattering angles for the three VLAD detector units and t_0 is an instrumental time offset

Parameter	Value
L_0	(11.055 ± 0.2) m
L_1	(2.013 ± 0.2) m
2θ	$(2 \pm 0.4)°$
	$(3.5 \pm 0.4)°$
	$(5 \pm 0.4)°$
t_0	(-6.1 ± 2.0) μs
E_1	(6671 ± 53) meV

3 Analysis and results

The H signal peaks in the TOF spectra can be analyzed to yield the O–H stretching band. The H signal peaks of Figs. 8–10 are in the form of histograms where the count rate per time bin can be expressed as

$$C(t) = \Phi(E_0) N_s \frac{\partial^2\sigma}{\partial\Omega\partial E_1}\, \eta(E_1)\, \delta t\, \delta E_1 \delta\Omega. \tag{6}$$

Here $\Phi(E_0)$ is the flux of neutrons of energy E_0 at the scattering sample, N_s is the number of scattering centers in the sample, $\frac{\partial^2\sigma}{\partial\Omega\partial E_1}$ is the sample double-differential scattering cross section, δE_1 is the total width of the nuclear resonance, η represents the detection efficiency and $\delta\Omega$ the detector solid angle.

The double-differential scattering cross section is related to the dynamic structure factor $S_q(\omega)$ via the equation:

$$S(q,\omega) = \frac{\boldsymbol{k_0}}{\boldsymbol{k_1}} \frac{4\pi}{\sigma_{\text{tot}}} \frac{\partial^2\sigma}{\partial\Omega\partial E_1}. \tag{7}$$

where $\boldsymbol{k_0}$ and $\boldsymbol{k_1}$ are the initial and final neutron wave vectors, respectively and $\sigma_{\rm tot} = \sigma_{\rm coh} + \sigma_{\rm inc}$ is the total (coherent plus incoherent) scattering cross section.

By combining (6)–(7) the scattering functions $S(q, \omega)$ can be determined from the $C(t)$ histograms of Figs. 7–9. This requires a change of variable from t to ω which is done using the relation:

$$\hbar\omega = \frac{1}{2} m \frac{L_0^2}{[t - t_r]^2} - E_1, \tag{8}$$

where E_1 is the resonance energy of the ^{238}U foil and $t_r = L_1\sqrt{(m/2E_1)}$.

Since $C(t)$ is a time histogram, the corresponding energy histogram is obtained by multiplying this quantity by $\left|\frac{\mathrm{d}(\hbar\omega)}{\mathrm{d}t}\right| = \left|\frac{-mL_0^2}{(t-t_r)^3}\right|$. In the end, the scattering functions $S(q, \omega)$ shown in Fig. 11 have been determined using the equation:

$$S_q(\omega) = \frac{\boldsymbol{k_0}}{\boldsymbol{k_1}} C(t)\,(t - t_r)^3 \times K \tag{9}$$

where

$$K = 4\pi \left(\Phi_{\rm target}(E_0)\, N_{\rm s}\, \eta(E_1), \delta E_1\, \delta\, \Omega\, \sigma_{\rm tot}\, m L_0^2\right)^{-1}. \tag{10}$$

Here q denotes the transferred wave vector, approximately constant for each detector, which is related to the scattering angle 2θ via [7]:

$$\frac{\hbar^2 q^2}{2m} = 2E_1 + \hbar\omega - 2\,\cos 2\theta \sqrt{E_1\,(E_1 + \hbar\omega)} \tag{11}$$

The q values corresponding to the transferred energies in the O–H stretching band (namely about 420 meV) were about 2.5 Å^{-1}, 4 Å^{-1}and 5.5 Å^{-1} for the three detectors. Given the point-to-point correspondence between the $C(t)$ data of Figs. 8–10 and the $S(q, \omega)$ histograms of Fig. 11, it is not surprising that the peaks due to the O–H stretching vibrational band of water are still visible on the right-hand side of the main H recoil peak.

An important point in the data analysis is the absolute normalization of $S(q, \omega)$. Not all the coefficients in (10) are known with good accuracy. These coefficients could be determined using a reference calibration sample, as done for instance in [12]. Unfortunately this was not possible in the present measurements. Instead, a comparison has been made with a simulation calculation performed with the DINSMS code, a neutron transport Monte Carlo code [15] which is used to simulate time of flight spectra for different samples investigated on the VESUVIO spectrometer. It also calculates multiple scattering and sample dimensions contributions to the resolution. DINSMS code is usually employed to simulate DINS measurements on VESUVIO, i.e. in the limit of high q, and based on impulse approximation (IA). The latter is valid for very high values of exchanged energy and momentum.

For the present measurement the code has been modified providing detector configuration routines accounting for the YAP RD operation, together with a suitable model dynamical structure factor for Ice Ih in the (q, ω) range of the present measurements. In particular, a model $S(q, \omega)$ was derived from [16] for the $\hbar\omega < 300$ meV range, and from [12] in the O–H stretching region (300 meV $< \hbar\omega <$ 600 meV),

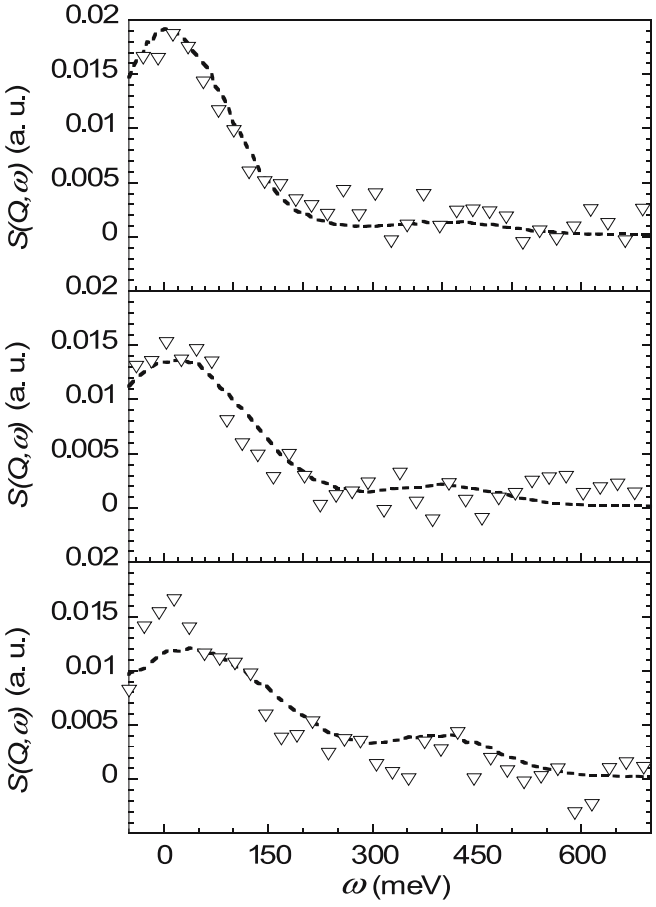

FIGURE 11 $S(q, \omega)$ for the three angles $2\theta = 2°$, 3.5° and 5° derived from data in Figs. 8–9. The O–H stretching band is located at about 417 meV to the right of the main recoil peak ($\hbar\omega \approx 0$ meV). The *dashed lines* are simulations as explained in the text

In Fig. 11 the experimental $S(q, \omega)$ for different angles is compared with the same scattering function from DINSMS simulations. The experimental data are normalised so as to give the same area of the $S(q, \omega)$ in the region -300 meV $< \hbar\omega < 300$ meV. The width of the H band below about 300 meV and the O–H stretching band, dominated by instrumental contributions, appear to be modelled correctly in the Monte Carlo simulation.

4 Density of states

A further step in the data analysis is to derive the H-projected density of states in the O–H stretching region, by performing the $q \to 0$ limit of the $S(q, \omega)$.

In polycrystalline samples $S(q, \omega)$ can be related [12, 17] to the density of states $g(\omega)$ by:

$$\lim_{q\to 0} \Gamma(q, \omega) \;=\; g(\omega) \tag{12}$$

where

$$\Gamma(q, \omega) = \left[\frac{S\,(q, \omega)}{q^2}\, \frac{2m\,\hbar\omega}{\mathrm{e}^{-2W}}\, \frac{4\pi}{\sigma_{\rm inc}}\, \frac{1}{n\,(\omega) + 1}\right] \tag{13}$$

where $n(\omega)$ is the Bose population factor (≈ 1 for T = 270 K) and e^{-2W} is the Debye–Waller factor. The latter is not far from

unity and was estimated from its $q \to 0$ limit [18]:

$$2W \approx \frac{1}{3} q^2 \langle u^2 \rangle , \tag{14}$$

where for $\langle u^2 \rangle$, the mean-square displacement of hydrogen nuclei from their equilibrium position, was assumed to have the value of $(0.484\ \text{Å})^2$, as reported in [19].

The relation (12) can be used to determine the shape and intensity of the $g(\omega)$ contribution due to the H-projected density of states in the O–H stretching region from the measured scattering functions, as done for instance in [12]. The energy range of interest is 350–500 meV, where the internal mode band (O–H stretching) is located. The shape of $g(\omega)$ as extrapolated in (12) is reported in Fig. 12.

The extrapolation is based on a fit of the form

$$\Gamma(q, \omega) = g(\omega) + \alpha q^2 \tag{15}$$

to each triplet of values (one for the q value of individual detectors) obtained from the data of Fig. 11. The error bars in Fig. 12 are the statistical uncertainties of the fit parameter $g(\omega)$.

On integrating $g(\omega)$,one obtains the number of stretching modes in the O–H stretching region. The result is:

$$\int_{350\ \text{meV}}^{450\ \text{meV}} g(\omega)\ \mathrm{d}\omega = 9 \pm 2. \tag{16}$$

This number has to be compared with the expected number $n = 8$ of stretching modes in a unit cell of ice Ih, in agreement with previous results (see e.g. [12]). The integration limits have been chosen so as to provide the correct result when applied to the simulation (see Fig. 11), and to take into account the overlapping of the O–H stretching peak with the elastic peak. Including a larger interval in the integration would result in a large overestimation of the integral (16) due to the contribution from the elastic peak tail underneath the O–H stretching peak. This approach is somewhat simplified but adequate for the purposes of this paper, especially considering the modest statistical quality of the data. The quoted error in the integral is purely statistical and is mainly due to the uncertainties arising from the background subtraction.

The instrumental energy resolution is the dominant contribution to the width of $g(\omega)$ in Fig. 12. It amounts to about 140 meV (FWHM) (in [20] 70 mm was erroneously misprinted as the FWHM instead of the HWHM). The modest quality of the data in Fig. 12 is clearly a consequence of coarse energy binning (due to the 0.5 μs binning in the measured TOF spectra) and, especially, poor statistics. All these will be improved when the full VLAD detector array becomes operational.

Despite the limited quality of the presented data it is possible to extract the "true" shape of $g(\omega)$. To this aim a Gaussian curve was fitted to the data in Fig. 12. An instrumental width of FWHM = 140 meV and Gaussian shape, as calculated in [8] was then subtracted in quadrature from the fitted Gaussian to provide the $g(\omega)$ curve shown in Fig. 12 as a dashed line. The resulting width is FWHM = 55 meV, i. e. much narrower than the instrumental energy resolution. Under these conditions, the demand for statistical accuracy become even higher. Only when the full VLAD array becomes available will it be possible to attain the data quality required to perform a quantitative shape analysis of $g(\omega)$.

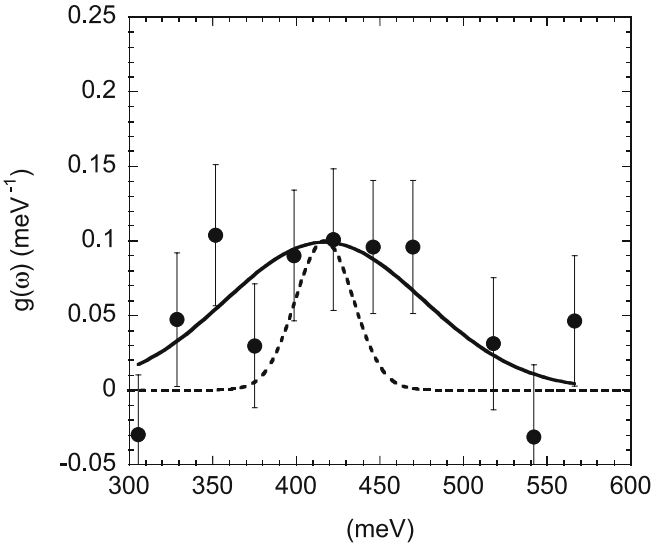

FIGURE 12 Extrapolated $g(\omega)$ as obtained from VLAD data. The *full line* is a Gaussian fit to the experimental data. The dashed Gaussian is the "true" $g(\omega)$ obtained by subtracting in quadrature the instrumental resolution contribution (see text)

5 Conclusions

A benchmark HINS experiment in an ice Ih sample has been performed with the new very low angle detector prototype of the VESUVIO spectrometer. It is the first time that this kind of measurement has been performed on an inverse geometry time-of-flight neutron spectrometer. The H-projected density of states in the stretching region have been derived, obtaining results in good agreement with the previous available data. Comparison between the experimental and simulated results $S(q, \omega)$ has shown that the data are compatible with $n = 9 \pm 2$ stretching modes. The technical solutions chosen for the VLAD prototype have proven to be well adapted to the challenge; data reduction techniques have also been defined. The VLAD prototype has shown that the RD is an effective technique for HINS, opening the way for a number of applications.

ACKNOWLEDGEMENTS This work was performed with financial support by the European Community contract HPRI-2001-50043 and within the CNR-CCLRC agreement. The authors acknowledge Consiglio Nazionale delle Ricerche (CNR)-Italy for financial support for the experiments performed at the ISIS pulsed neutron source.

REFERENCES

1 A.D. Taylor, R. Osborn, K.A. McEwan, G.W. Stirling, Z.A. Bodwen, W.G. Williams, E. Balcar, S.W. Lovesey, Phys. Rev. Lett. **61**, 1309 (1988)
2 G. Amoretti, A. Blaise, R. Caciuffo, J.M. Fournier, M.T. Hutchings, R. Osborn, A.D. Taylor, Phys. Rev. B **40**, 1856 (1989)
3 J.F. Cooke, J.A. Blackman, Phys. Rev. B **26**, 4410 (1982)
4 T. Morgan, J.A. Blackman, J.F. Cooke, Phys. Rev. B **33**, 7154 (1986)

5 G. Gorini E. Perelli-Cippo, M. Tardocchi, C. Andreani, A. D'Angelo, A. Pietropaolo, R. Senesi, S. Imberti, A. Bracco, E. Previtali, G. Pessina, N.J. Rhodes, E.M. Schooneveld, Nucl. Instrum. Methods A **529**, 293 (2004)

6 R. Senesi, C. Andreani, Z. Bowden, D. Colognesi, E. Degiorgi, A.L. Fielding, J. Mayers, M. Nardone, J. Norris, M. Praitano, N.J. Rhodes, W.G. Stirling, J. Tomkinson, C. Uden, Physica B **276–278**, 200 (2000)

7 C.G. Windsor, *Pulsed Neutron Scattering* (Taylor and Francis, London, 1981)

8 S. Imberti, C. Andreani, V. Garbuio, G. Gorini, A. Pietropaolo, R. Senesi, M. Tardocchi, Nucl. Instrum. Methods A **552**, 463 (2005)

9 M. Tardocchi A. Pietropaolo, C. Andreani, G. Gorini, E. Perelli-Cippo, N.J. Rhodes, E.M. Schooneveld, R. Senesi, Nucl. Instrum. Methods A **535** 121 (2004)

10 E. Perelli-Cippo, G. Gorini, M. Tardocchi, O. Cremonesi, C. Andreani, A. Pietropaolo, R. Senesi, Z.A. Bodwen, N.J. Rhodes, E.M. Schooneveld, Transact. Nucl. Sci. **52**, No. 4, 1092 (2005)

11 M. Tardocchi, G. Gorini, A. Pietropaolo, C. Andreani, R. Senesi, N.J. Rhodes, E.M. Schooneveld, Rev. Sci. Instrum. **75**, 4880 (2004)

12 C. Andreani, P. Bosi, F. Sacchetti, C.K. Loong, J. Chem. Phys. **83**, 750 (1985)

13 M.A. Ricci, M. Nardone, A. Fontana, C. Andreani, W. Hahn, J. Chem. Phys. **108**, 450 (1998)

14 A. Pietropaolo, C. Andreani, A. Filabozzi, R. Senesi, G. Gorini, E. Perelli-Cippo, M. Tardocchi, N.J. Rhodes, E.M. Schooneveld, Appl. Phys. A (2006), submitted

15 J. Mayers, A.L. Fielding, R. Senesi, Nucl. Instrum. Methods A **481**, 454 (2002)

16 A.I. Kolesnikov, J. Li, S.F. Parker, R.S. Eccleston, C.K. Loong, Phys. Rev. B **59**, 3569 (1999)

17 S.W. Lovesey, *Theory of Neutron Scattering from Condensed Matter*, Vol. 1 (London, Oxford University Press, 1987)

18 K. Toukan, M.A. Ricci, S.H. Chen, C.K. Loong, D.L. Price, J. Texeira, Phys. Rev. A **37**, 2580 (1988)

19 J. Teixeira, M.C. Bellissent-Funel, S.H. Chen, A.J. Dianoux, Phys. Rev. A **31**, 1913 (1985)

20 C. Andreani, A. Pietropaolo, R. Senesi, G. Gorini, E. Perelli-Cippo, M. Tardocchi, N. Rhodes, E.M. Schooneveld, Appl. Phys. Lett. **85**, 5454 (2004)